Article

Controllable and Repeatable Synthesis of Thermally Stable Anatase Nanocrystal–Silica Composites with Highly Ordered Hexagonal Mesostructures

Weiyang Dong, Yaojun Sun, Chul Wee Lee, Weiming Hua, Xinchun Lu, Yifeng Shi, Shicheng Zhang, Jianmin Chen, and Dongyuan Zhao

J. Am. Chem. Soc., **2007**, 129 (45), 13894-13904• DOI: 10.1021/ja073804o • Publication Date (Web): 17 October 2007

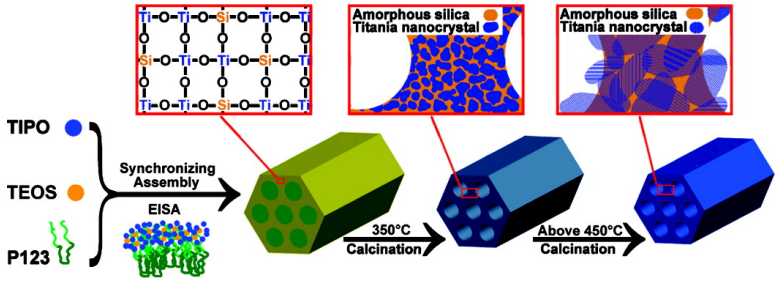

More About This Article

Additional resources and features associated with this article are available within the HTML version:

- Supporting Information
- Links to the 5 articles that cite this article, as of the time of this article download
- Access to high resolution figures
- Links to articles and content related to this article
- Copyright permission to reproduce figures and/or text from this article

View the Full Text HTML

J|A|C|S
ARTICLES
Published on Web 10/17/2007

Controllable and Repeatable Synthesis of Thermally Stable Anatase Nanocrystal−Silica Composites with Highly Ordered Hexagonal Mesostructures

Weiyang Dong,*,† Yaojun Sun,§ Chul Wee Lee,|| Weiming Hua,‡ Xinchun Lu,§ Yifeng Shi,‡ Shicheng Zhang,† Jianmin Chen,† and Dongyuan Zhao*,‡

Contribution from the Department of Environmental Science and Engineering, Center for Analysis and Measurement, and Department of Chemistry, Fudan University, 220 Handan Road, Shanghai 200433, P. R. China, and Advanced Chemical Technology Division, Korea Research Institute of Chemical Technology, P.O. Box 107, Yuseong, Daejeon 305-600, Korea

Received May 25, 2007; E-mail: dyzhao@fudan.edu.cn; wydong@fudan.edu.cn

Abstract: In this article, we report a controllable and reproducible approach to prepare highly ordered 2-D hexagonal mesoporous crystalline TiO_2-SiO_2 nanocomposites with variable Ti/Si ratios (0 to ∞). XRD, TEM, and N_2 sorption techniques have been used to systematically investigate the pore wall structure, and thermal stability functioned with the synthetic conditions. The resultant materials are ultra highly stable (over 900 °C), have large uniform pore diameters (~6.8 nm), and have high Brunauer−Emmett−Teller specific surface areas (~290 m^2/g). These mesostructured TiO_2-SiO_2 composites were obtained using titanium isopropoxide (TIPO) and tetraethyl orthosilicate (TEOS) as precursors and triblock copolymer P123 as a template based on the solvent evaporation-induced co-self-assembly process under a large amount of HCl. Our strategy was the synchronous assembly of titanate and silicate oligomers with triblock copolymer P123 by finely tuning the relative humidity of the surrounding atmosphere and evaporation temperature according to the Ti/Si ratio. We added a large amount of acidity to lower condensation and polymerization rates of TIPO and accelerate the rates for TEOS molecules. TEM and XRD measurements clearly show that the titania is made of highly crystalline anatase nanoparticles, which are uniformly embedded in the pore walls to form the "bricked-mortar" frameworks. The amorphous silica acts as a glue linking the TiO_2 nanocrystals and improves the thermal stability. As the silica contents increase, the thermal stability of the resulting mesoporous TiO_2-SiO_2 nanocomposites increases and the size of anatase nanocrystals decreases. Our results show that the unique composite frameworks make the mesostructures overwhelmingly stable; even with high Ti/Si ratios (≥80/20) the stability of the composites is higher than 900 °C. The mesoporous TiO_2-SiO_2 nanocomposites exhibit excellent photocatalytic activities (which are higher than that for commercial catalyst P25) for the degradation of rhodamine B in aqueous suspension. The excellent photocatalytic activities are ascribed to the bifunctional effect of highly crystallized anatase nanoparticles and high porosity.

Introduction

Titania-based materials have attracted much attention because of their unique electronic and optical properties and potential applications in photocatalysis, chemical sensing and energy conversion, solar cells, advanced battery, and even water purification.[1−5] It is known that the properties of titania-based materials strongly depend on their crystallinity and surface property;[1b] high surface areas are always desired.[3] The reports of mesoporous silicates M41S throw a light on the preparation of high surface area TiO_2-based materials.[6−22] Although an efficient method via evaporation-induced self-assembly (EISA) process is adopted to prepare ordered mesoporous titania,[7−12]

† Department of Environmental Science and Engineering, Fudan University.
§ Center for Analysis and Measurement, Fudan University.
|| Advanced Chemical Technology Division, Korea Research Institute of Chemical Technology.
‡ Department of Chemistry, Fudan University.

(1) (a) Hagfeldt, A.; Gratzel, M. *Chem. Rev.* **1995**, *95*, 49−68. (b) Kawahara, T.; Konishi, Y.; Tada, H.; Tohge, N.; Nishii, J.; Ito, S. *Angew. Chem., Int. Ed.* **2002**, *41*, 2811−2813. (c) Asahi, R.; Morikawa, T.; Ohwaki, T.; Aoki, K.; Taga, Y. *Science* **2001**, *293*, 269−271. (d) Hashimoto, K.; Irie, H.; Fujishima, A. *Jpn. J. Appl. Phys.* **2005**, *44*, 8269−8285.
(2) Qi, Z. M.; Honma, I.; Zhou, H. S. *Anal. Chem.* **2005**, *77*, 1163−1166.
(3) Zukalová, M.; Zukal, A.; Kavan, L.; Nazeeruddin, M. K.; Liska, P.; Grätzel, M. *Nano Lett.* **2005**, *5*, 1789−1792.
(4) Zou, X. J.; Maesako, N.; Nomiyama, T.; Horie, Y.; Miyazaki, T. *Sol. Energy Mater. Sol. Cells* **2000**, *62*, 133−142.
(5) Lettmann, C.; Hinrichs, H.; Maier, W. F. *Angew. Chem., Int. Ed.* **2001**, *40*, 3160−3164.
(6) (a) Kresge, C. T.; Leonowicz, M. E.; Roth, W. J.; Vartuli, J. C.; Beck, J. S. *Nature* **1992**, *359*, 710−712. (b) Beck, J. S.; Vartuli, J. C.; Roth, W. J.; Leonowicz, M. E.; Kresge, C. T.; Schmitt, K. D.; Chu, C. T.-W.; Olson, D. H.; Sheppard, E. W.; McCullen, S. B.; Higgins, J. B.; Schlenker, J. L. *J. Am. Chem. Soc.* **1992**, *114*, 10834−10843.
(7) (a) Yang, P. D.; Zhao, D. Y.; Margolese, D. I.; Chmelka, B. F.; Stucky, G. D. *Nature* **1998**, *396*, 152−155. (b) Yang, P. D.; Zhao, D. Y.; Margolese, D. I.; Chmelka, B. F.; Stucky, G. D. *Chem. Mater.* **1999**, *11*, 2813−2826. (c) Bartl, M. H.; Puls, S. P.; Tang, J.; Lichtenegger, H. C.; Stucky, G. D. *Angew. Chem., Int. Ed.* **2004**, *43*, 3037−3040. (d) Alberius, P. C. A.; Frindell, K. L.; Hayward, R. C.; Kramer, E. J.; Stucky, G. D.; Chmelka, B. F. *Chem. Mater.* **2002**, *14*, 3284−3294.

 10.1021/ja073804o CCC: $37.00

compared to the flexible synthesis of the silicates, it is much more difficult to obtain mesoporous titania with ordered structures, large pore size, and high surface area because of an uncontrollable sol−gel process from a too fast hydrolysis−condensation rate.[10−12]

Because the formation is kinetically controlled and greatly influenced by the atmospheric conditions of the laboratory, the reproducibility in obtaining high-quality mesoporous titania is still a challenge.[10] It should be pointed out that the traditional ethanolic EISA approach has a drawback that the ordered mesoporous titania-based materials are only obtained for a narrow range of synthetic conditions such as temperature or relative humidity, which can be varied from laboratory to laboratory.[10] It is known that four variables should be carefully controlled during the EISA process:[11] (a) the water amount, (b) the relative humidity, (c) the evaporation rate, (d) the deposition and aging temperature, and so forth. However, the media acidity, which is very important for the polymerization and cross-linking of titanate oligomers, was lost sight of. Therefore, the indiscriminate condensation that takes place in low acidic medium can hinder the disorder-to-order transition before the formation of mesophases, "freezing" intermediate disordered phases.[11]

Another important issue that should be considered is the thermal stability of titania mesostructures. In most cases, the mesostructures collapse and lose most of the porosity after being heated at 300−350 °C because of the intrinsical crystallization of anatase phase.[9,10] Many attempts have been made to improve their thermal stabilities.[9−14] Khushalani et al. reported a post-treatment method by a mild silanation with Si_2H_6 under a vacuum condition; however, this improvement could not make the TiO_2 mesostructure be stable at higher than 500 °C because of too-thin silicate layers.[13] Sanchez and co-workers[11,12] reported that the mesoporous anatase networks could be stable at 650 °C by applying a postsynthesis delayed rapid crystallization treatment. Ozin and co-workers tried to form a thick wall to improve the stability.[10] They added butanol in triblock copolymer P123 templating system to promote the formation of thick pore walls with large pores. However, the calcination at above 400 °C resulted in the destruction of the mesostructure.

An alternative route to resolve the stability problem is to add the amorphous components such as P_2O_5, SiO_2, or carbon into the mesostructured TiO_2 frameworks, which can form a random glasslike network and is responsible for the stability of ordered mesostructure.[9] Zhou and co-workers studied the synthesis and structure of ordered mesostructured $TiO_2-P_2O_5$ composites.[9] They found that the amorphous P_2O_5 serves as a glass phase to stick TiO_2 nanocrystals in the mesostructured frameworks, resulting in a great improvement of their thermal stabilities (up to 700 °C). However, the formation temperature of anatase crystallites also greatly increases because of the strong interaction between P_2O_5 and TiO_2.[9] Although they claimed that the ordered mesostructured TiO_2-SiO_2 composite can also be obtained, detailed reports on the synthesis and structures have not been given yet.[9]

In this article, we report a controllable and reproducible approach to synthesize thermally stable TiO_2-SiO_2 composites with variable Ti/Si ratios (0 to ∞) based on an ethanolic EISA process by using titanium isopropoxide (TIPO) and tetraethyl orthosilicate (TEOS) as precursors and triblock copolymer P123 as a template. Our strategy is the synchronous assembly of titanate and silicate oligomers with triblock copolymer P123 by adding a large amount of HCl acidity. We also finely tuned the relative humidity of the surrounding atmosphere and evaporation temperature according to the Ti/Si ratio to control the polymerization rate of titanates and silicates and to lower the co-self-assembly process. Under such a condition, highly ordered two-dimensional (2-D) hexagonal mesostructured crystalline anatase−silica composites with large uniform pore sizes and high surface areas can easily be obtained in a wide range. It is a feature that the TiO_2 existed as anatase nanocrystals in the amorphous silica frameworks, and it is uniformly distributed on the surface in the pore walls. This unique composite framework with the "bricked mortar" structure brings the TiO_2 mesostructures overwhelming thermal stability (>900 °C). The mesoporous TiO_2-SiO_2 nanocomposites exhibit higher photocatalytic activities for the degradation of rhodamine B (RhB) in aqueous suspension, compared with that from commercial photocatalyst P25.

Experimental Section

Chemicals. Titanium isopropoxide [$Ti(OCH(CH_3)_2)_4$, TIPO] and tetraethyl orthosilicate [$Si(OC_2H_5)_4$, TEOS] were purchased from Fluka. Triblock poly(ethylene oxide)-*b*-poly(propylene oxide)-*b*-poly(ethylene oxide) copolymer, Pluronic P123 [$M_w = 5800$, $HO(CH_2CH_2O)_{20}(CH_2CHCH_3O)_{70}(CH_2CH_2O)_{20}H$, $EO_{20}PO_{70}EO_{20}$, abbreviated as P123], was received from Aldrich. Ethanol (absolute) and concentrated HCl (36.5 wt %) were purchased from Shanghai Chemical Corp. P25 (a commercial nanocrystalline TiO_2 consisting of ca. 80% anatase and 20% rutile; Brunauer−Emmett−Teller (BET) area is ca. 50 $m^2\ g^{-1}$) was supplied by Degussa Corp. RhB ($C_{28}H_{31}ClN_2O_3$), bought from Sigma-Aldrich, was prepared into 1×10^{-5} M aqueous solution with deionized water. All the chemicals were used as received without further purification.

Preparation. The highly ordered 2-D hexagonal mesoporous TiO_2-SiO_2 composites were synthesized via a solvent EISA method under a large amount of HCl and ethanol, by using TIPO and TEOS as the precursors and triblock copolymer P123 as a structure-directing agent. The composition of Ti/Si/H_2O/HCl/P123/EtOH (molar ratio) was varied

(8) (a) Tian, B. Z.; Liu, X. Y.; Tu, B.; Yu, C. Z.; Fan, J.; Wang, L. M.; Xie, S. H.; Stucky, G. D.; Zhao, D. Y. *Nat. Mater.* **2003**, *2*, 159−163. (b) Tian, B. Z.; Yang, H. F.; Liu, X. Y.; Xie, S. H.; Yu, C. Z.; Fan, J.; Tu, B.; Zhao, D. Y. *Chem. Commun.* **2002**, 1824−1825. (c) Xu, X.; Tian, B. Z.; Kong, J. L.; Zhang, S.; Liu, B. H.; Zhao, D. Y. *Adv. Mater.* **2003**, *15*, 1932−1936.
(9) Li, D. L.; Zhou, H. S.; Honma, I. *Nat. Mater.* **2004**, *3*, 65−72.
(10) Choi, S. Y.; Mamak, M.; Coombs, N.; Chopra, N.; Ozin, G. A. *Adv. Funct. Mater.* **2004**, *14*, 335−344 and references therein.
(11) Crepaldi, E. L.; Soler-Illia, G. J. de A. A.; Grosso, D.; Cagnol, F.; Ribot, F.; Sanchez, C. *J. Am. Chem. Soc.* **2003**, *125*, 9770−9786.
(12) (a) Soler-Illia, G. J. de A. A.; Scolan, E.; Louis, A.; Albouy, P. A.; Sanchez, C. *New J. Chem.* **2001**, *25*, 156−165. (b) Grosso, D.; Soler-Illia, G. J. de A. A.; Babonneau, F.; Sanchez, C.; Albouy, P. A.; Brunet-Bruneau, A.; Balkenende, A. R. *Adv. Mater.* **2001**, *13*, 1085−1090. (c) Soler-Illia, G. J. de A. A.; Louis, A.; Sanchez, C. *Chem. Mater.* **2002**, *14*, 750−759. (d) Crepaldi, E. L.; Soler-Illia, G. J. de A. A.; Grosso, D.; Sanchez, C. *New J. Chem.* **2003**, *27*, 9−13.
(13) Khushalani, D.; Ozin, G. A.; Kuperman, A. *J. Mater. Chem.* **1999**, *9*, 1491−1500.
(14) Lyu, Y. Y.; Yi, S. H.; Shon, J. K.; Chang, S.; Pu, L. S.; Lee, S. Y.; Yie, J. E.; Char, K.; Stucky, G. D.; Kim, J. M. *J. Am. Chem. Soc.* **2004**, *126*, 2310−2311.
(15) Antonelli, D. M.; Ying, J. Y. *Angew. Chem., Int. Ed.* **1995**, *34*, 2014−2017.
(16) Stone, V. F., Jr.; Davis, R. J. *Chem. Mater.* **1998**, *10*, 1468−1474.
(17) Trong On, D. *Langmuir* **1999**, *15*, 8561−8564.
(18) Perkas, N.; Palchik, O.; Brukental, I.; Nowik, I.; Gofer, Y.; Koltypin, Y.; Gedanken, A. *J. Phys. Chem. B* **2003**, *107*, 8772−8778.
(19) Liu, P.; Liu, J.; Sayari, A. *Chem. Commun.* **1997**, 577−578.
(20) (a) Antonelli, D. M. *Microporous Mesoporous Mater.* **1999**, *30*, 315−319. (b) Murray, S.; Trudeau, M.; Antonelli, D. M. *Inorg. Chem.* **2000**, *39*, 5901−5908. (c) Ye, B.; Trudeau, M.; Antonelli, D. *Chem. Mater.* **2001**, *13*, 2730−2741.
(21) Yun, H. S.; Miyazawa, K.; Zhou, H. S.; Honma, I.; Kuwabara, M. *Adv. Mater.* **2001**, *13*, 1377−1380.
(22) Liu, C.; Fu, L.; Economy, J. *J. Mater. Chem.* **2004**, *14*, 1187−1189.

in the range of (1−0.6):(0−0.4):(5.25−10.5):(1.5−3.0):(0.014−0.021):(43−65). The relative humidity required in the surrounding atmosphere during the solvent evaporation was finely tuned and strictly controlled in the range of 50−100%. The obtained samples were assigned to xTiO$_2$−(100 − x)SiO$_2$, where x represents molar percentage of TiO$_2$.

For a typical synthesis, 1.0 g of copolymer P123 was dissolved in 30 g of ethanol, then 1.8 g of concentrated HCl was slowly added with vigorous stirring. After being heated in a sealed bottle at 40 °C for 3 h, 2.34 g of TIPO and 0.434 g of TEOS were added with vigorous stirring for 5 h at 40 °C. The sols were transferred into Petri dishes and evaporated at 35 °C in air with relative humidity of 50−60% for about 4 days, and the resulting transparent membranes were dried at 80 °C for 6 days. The samples were calcined at 350 or 400 °C for 6 h in air to remove organic templates and subsequently heated at 450−900 °C for 2−4 h in air with the heating rate of 1 °C/min. The final products (80TiO$_2$−20SiO$_2$) were obtained.

For comparison, the pure TiO$_2$ mesostructure was prepared in a similar procedure. P123 (1.0 g) was dissolved in 30 g of ethanol and 3.0 g of concentrated HCl with vigorous stirring. After being heated at 40 °C for 3 h, 3.0 g of TIPO was added with vigorous stir for 20 h at 40 °C. The solution was poured into the dishes and evaporated at 35 °C in air and 50−60% relative humidity for about 5 days, and the resulting membranes were dried at 80°C for 7 days. The samples were calcined at 350 °C for 6 h in air to remove organic templates and subsequently heated at 400−450 °C for 2 h in air.

Mesoporous silica was also prepared using a similar procedure. P123 (1.0 g) was dissolved in 20 g of ethanol containing 1.2 g of 4 M HCl with vigorous stirring. After being heated in a sealed bottle at 40 °C for 2 h, 2.2 g of TEOS was added with stirring for 4 h at 40 °C. The sols were transferred into the dishes and dried at 40 °C for 3 days (80−100% relative humidity). The obtained transparent membranes were calcined at 400 °C for 6 h and then further heated at 450−900 °C for 4 h in air.

Characterization. Small-angle X-ray powder diffraction (SAXRD) patterns were recorded on a German Bruker D4 X-ray diffractometer with Ni-filtered Cu Kα radiation (40 kV, 40 mA). Wide-angle X-ray diffraction (WAXRD) patterns were collected on a Rigaku D/MAX-rB X-ray powder diffractometer using a high-power Cu Kα (λ = 0.15418 nm) source operating at 40 kV and 60 mA with a graphite monochromator filter. The size of anatase nanocrystals was estimated by using the Scherrer equation to the half-height width of the 101 diffraction peak with silicon as a standard for the instrumental line broadening. Transmission electron microscopy (TEM) images and high-resolution TEM (HRTEM) images were obtained on a JEM-2011 transmission electron microscope (JEOL Company) combined with energy-dispersive X-ray spectroscopy operating at 200 kV. For TEM measurements, the samples were prepared by sonication in ethanol and suspended on holey carbon grids. N$_2$ adsorption−desorption isotherms were collected on a Micromeritics ASAP 2010 adsorption analyzer at −196 °C (77 K). All samples were degassed at 250 °C for at least 5 h before analyses. The BET specific surface areas were calculated from adsorption data at a relative pressure range from 0.057 to 0.20. The total pore volumes (V_T) were calculated at a relative pressure of 0.976. Mesopore size distributions were calculated from adsorption branches using the Barrett−Joyner−Halenda (BJH) method. ^{29}Si solid-state magic-angle spinning (MAS) NMR experiments were performed at room temperature on a Bruker DSX 300 spectrometer at a resonance frequency of 59.63 MHz and a radiation frequency intensity of 52 kHz with a 7.0-mm MAS probe. The samples were packed in 7-mm zirconia rotors fitted with Kel-F end caps for MAS of 4 kHz. Single pulse MAS NMR spectra were recorded with a 60° pulse of 3.2 μs and a recycle delay of 300 s. Chemical shifts were determined with respect to Q_8M_8 as an external standard at δ = 12.6 ppm.

The photocatalytic activities were evaluated by RhB decomposition under UV light irradiation from a 25 W Hg lamp (λ = 254 nm). The radiant flux was measured with a photometer (International Light model IL1400A). Aqueous suspensions (50 mL) of RhB (1×10^{-5} M) and the composite powder sample (1.00 g L^{-1}) were placed in a quartz vessel. Before irradiation, the suspensions were stirred in the dark for 30 min to establish the adsorption−desorption equilibrium between RhB and the sample surface. At given time intervals, the supernates were analyzed by recording the variations of the absorption band maximum (554 nm) using a ThermoSpectronic UV 500 UV−visible spectrometer. For comparison, the weight of all the samples tested for the activity was controlled to be exactly same (50.0 mg).

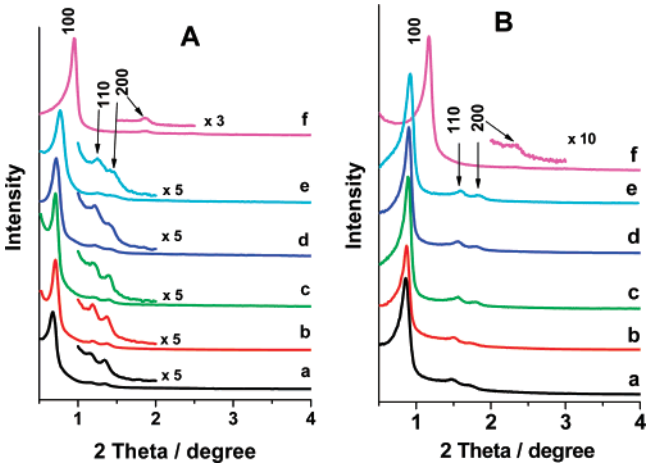

Figure 1. SAXRD patterns of the as-synthesized (A) and calcined (B) ordered hexagonal mesostructured TiO$_2$−SiO$_2$ composites with varied Ti/Si ratios: (a) pure TiO$_2$, (b) 90TiO$_2$−10SiO$_2$, (c) 80TiO$_2$−20SiO$_2$, (d) 70TiO$_2$−30SiO$_2$, (e) 60TiO$_2$−40SiO$_2$, and (f) pure SiO$_2$. The calcination was carried out in air at 350 °C for 6 h for mesoporous TiO$_2$ (a); 450 °C for 4 h for 90TiO$_2$−10SiO$_2$ (b), 80TiO$_2$−20SiO$_2$ (c), 70TiO$_2$−30SiO$_2$ (d), and 60TiO$_2$−40SiO$_2$ (e); and 600 °C for 4 h for mesoporous SiO$_2$ (f).

Results and Discussion

Mesoporous Titania. Highly ordered mesoporous titania can be easily synthesized via a solvent EISA method under a large amount of HCl in a wide range by using TIPO as a titanium source and triblock copolymer P123 as a template. The SAXRD pattern (Figure 1Aa) of as-synthesized mesoporous TiO$_2$ product shows three well-resolved diffraction peaks with d-spacing ratios of 1:$\sqrt{3}$:2 at 2θ angle of 0.5−2.0°, which can be indexed as the 100, 110, and 200 reflections of typical 2-D hexagonal mesostructure (space group of $p6mm$),[7a,8a,9,10] respectively. It clearly indicates that a highly ordered mesostructured TiO$_2$ with the cell parameter (a_0) of 15.0 nm is obtained (Table 1). After being calcined at 350 °C for 6 h in air to remove the organic template, three resolved diffraction peaks can also be observed (Figure 1Ba), indicating that the highly ordered 2-D hexagonal mesostructure is stable. The unit cell (a_0) is calculated to be 11.9 nm, suggesting a large shrinkage of 20.7%. After being calcined at 400 °C, the XRD pattern becomes poor, the diffractions slightly shift to high angles (Supporting Information, Figure S1), and a further shrinkage (5.4%) is observed. After being calcined at 450 °C for 2 h in air, the XRD pattern becomes poorer and only one weak diffraction peak is observed, suggesting that the mesostructure is greatly degraded. Another minor structural shrinkage (2.4%) is observed. The results show that the TiO$_2$ mesostructure can be thermally stable in 400−450 °C, which is coincident with previous reports.[9,10] It is mainly related to the growth and coarsening of the anatase nanocrystallites.[9] This is further confirmed by the TEM observations.

Table 1. Physicochemical Properties of the Mesoporous TiO_2-SiO_2 Composites Prepared with Different Ti/Si Ratios and Calcining Temperatures

sample name	temp and time of cal °C (h)[a]	a_0 nm	mean pore size[b] nm	S_{BET}[c] $m^2\ g^{-1}$	V_T[d] mL g^{-1}	HHW-PSD[e] nm	average nanocrystal size[f] nm	average thickness of pore walls[g] nm
TiO_2-0	as-made	15.0						
TiO_2-1	350 (6)	11.9	7.6	271	0.38	0.76	6.0 (7.0)	4.3 (3.8)
TiO_2-2	400 (2)	11.1	6.3	213	0.34	0.81	6.5	4.8
TiO_2-3	450 (2)	10.7	5.7	171	0.26	2.33	7.7 (10.4)	5.0 (5.2)
$90TiO_2-10SiO_2$-0	as-made	14.8						
$90TiO_2-10SiO_2$-1	450 (4)	11.9	7.1	292	0.43	0.74	4.9	4.8
$90TiO_2-10SiO_2$-2	500 (4)	11.8	7.0	270	0.40	0.79	5.6 (8.5)	4.8 (5.3)
$90TiO_2-10SiO_2$-3	550 (4)	11.8	7.0	256	0.38	0.79	5.9	4.8
$90TiO_2-10SiO_2$-4	600 (4)	11.7	6.8	233	0.35	0.81	6.3	4.9
$90TiO_2-10SiO_2$-5	650 (4)	11.4	6.5	218	0.33	0.81	6.9	4.9
$90TiO_2-10SiO_2$-6	700 (2)	11.3	6.3	202	0.30	0.94	7.8 (10)	5.0 (5.0)
$90TiO_2-10SiO_2$-7	750 (2)	10.6	5.4	170	0.23	2.00	8.9	5.2
$80TiO_2-20SiO_2$-0	as-made	14.3						
$80TiO_2-20SiO_2$-1	600 (4)	11.4	6.7	251	0.35	0.76	6.0	4.7
$80TiO_2-20SiO_2$-2	650 (4)	11.2	6.5	236	0.33	0.79	6.4	4.7
$80TiO_2-20SiO_2$-3	700 (4)	11.0	6.2	219	0.29	0.79	7.0 (10)	4.8 (4.9)
$80TiO_2-20SiO_2$-4	750 (2)	10.7	5.9	204	0.27	0.79	7.7	4.8
$80TiO_2-20SiO_2$-5	800 (2)	10.6	5.8	190	0.25	0.84	8.7	4.8
$80TiO_2-20SiO_2$-6	850 (2)	10.4	5.5	175	0.22	0.95	9.4	4.9
$80TiO_2-20SiO_2$-7	900 (2)	9.4	4.4	73	0.08	1.85	12.5 (13)	5.0 (5.2)
$70TiO_2-30SiO_2$-0	as-made	14.0						
$70TiO_2-30SiO_2$-1	600 (4)	11.2	6.6	278	0.35	0.73	4.9	4.6
$70TiO_2-30SiO_2$-2	650 (4)	11.0	6.4	246	0.32	0.77	6.0	4.6
$70TiO_2-30SiO_2$-3	700 (4)	10.9	6.2	230	0.30	0.78	6.3 (6.9)	4.7 (4.7)
$70TiO_2-30SiO_2$-4	750 (2)	10.6	5.8	223	0.29	0.78	6.8	4.8
$70TiO_2-30SiO_2$-5	800 (2)	10.5	5.7	217	0.28	0.81	7.5 (9.5)	4.8 (4.5)
$70TiO_2-30SiO_2$-6	850 (2)	10.4	5.5	198	0.25	0.91	8.3	4.9
$70TiO_2-30SiO_2$-7	900 (2)	9.6	4.7	128	0.14	1.50	10.3	4.9
$60TiO_2-40SiO_2$-0	as-made	13.3						
$60TiO_2-40SiO_2$-1	600 (4)	11.1	6.6	308	0.35	0.76	4.1	4.5
$60TiO_2-40SiO_2$-2	650 (4)	10.9	6.3	275	0.31	0.81	5.2	4.6
$60TiO_2-40SiO_2$-3	700 (4)	10.7	6.1	252	0.30	0.81	5.7	4.6
$60TiO_2-40SiO_2$-4	750 (2)	10.5	5.8	247	0.29	0.85	6.0	4.7
$60TiO_2-40SiO_2$-5	800 (2)	10.4	5.6	231	0.27	0.90	6.7 (7.8)	4.8 (4.4)
$60TiO_2-40SiO_2$-6	850 (2)	10.3	5.4	212	0.25	0.94	7.4	4.9
$60TiO_2-40SiO_2$-7	900 (2)	9.9	5.0	162	0.18	1.27	8.2	4.9
SiO_2-0	as-made	10.6						
SiO_2-1	600 (4)	8.7	3.9	426	0.35	0.67		4.8

[a] Temp and time of cal: Temperature and time of calcination. [b] Mean pore size: The mean pore size was calculated using the BJH method from the adsorption data of N_2 isotherms. [c] S_{BET}: BET specific surface area. [d] V_T: Total pore volume. [e] HHW-PSD: Half-height width of pore size distribution. [f] Average nanocrystal size: Calculated from the half-height width of the 101 diffraction peak on the WAXRD pattern using the Scherrer equation; the values in the parentheses were obtained by measuring the size of the nanocrystals from the TEM images. [g] Average thickness of pore walls: Obtained from a_0 minus the mean pore size; the values in the parentheses were obtained by measuring the thickness of the pore walls from the TEM images.

The WAXRD pattern (Figure 2a) of mesoporous TiO_2 structure calcined at 350 °C in air shows broad diffraction peaks of anatase phase,[7a,9,10] suggesting a formation of TiO_2 nanocrystallites. With the increase in calcination temperature, the diffraction peaks become strong and narrow (Figure S2), suggesting a growth in TiO_2 crystallinity. According to Scherrer's method, the size of anatase nanocrystals increases from 6.0 to 7.7 nm (Table 1).

TEM images viewed along the [001] and [110] directions further confirm that mesoporous TiO_2 products calcined at 350 °C (Figure 3a,b) have a highly ordered 2-D hexagonal regularity. The a_0 evaluated from TEM measurements is 11.6 nm, which is consistent with the value calculated from SAXRD patterns (Table 1). HRTEM images (Figure 3c,d) reveal that anatase nanocrystals are clearly embedded in the matrix of the pore walls with random orientation. Some amorphous TiO_2 can also be observed in the pore walls. The average *d*-spacing of the lattice fringes measured from the TEM images is about 0.34 nm, agreeing with the d_{101} value of 0.35 nm calculated from the corresponding WAXRD patterns. The size of anatase nanocrystals evaluated from the TEM images is about 7.0 nm, which is a little larger than the value calculated from WAXRD patterns. Some of the anatase nanocrystals pierce into the mesochannels; however, they are still glued and linked with amorphous TiO_2 mortars, suggesting a formation of the "bricked mortar" framework structure. The average pore wall thickness evaluated is about 3.8 nm, which is a little smaller than that calculated from XRD and N_2 sorption data. As the calcination temperature increases to 450 °C, TEM images show that the regularity of mesoporous TiO_2 product becomes poor (Figure S3). However, the ordered hexagonal arrays with clear defects are still observed in a large domain from the TEM images (Figure S3). The dense, randomly oriented large anatase nanocrystallites, which grow from the pore walls and block the channels, can be clearly seen.

N_2 adsorption−desorption isotherms of 2-D hexagonal mesoporous TiO_2 calcined at 350 °C show typical type IV curves with a sharp capillary condensation step at relative pressure (*p*/

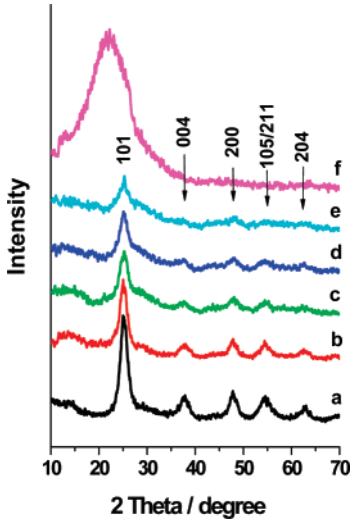

Figure 2. WAXRD patterns of (a) mesoporous TiO_2 calcined at 350 °C for 6 h; (b) mesoporous $90TiO_2-10SiO_2$, (c) $80TiO_2-20SiO_2$, (d) $70TiO_2-30SiO_2$, and (e) $60TiO_2-40SiO_2$ composites calcined at 450 °C for 4 h; and (f) mesoporous silica calcined at 600 °C for 4 h.

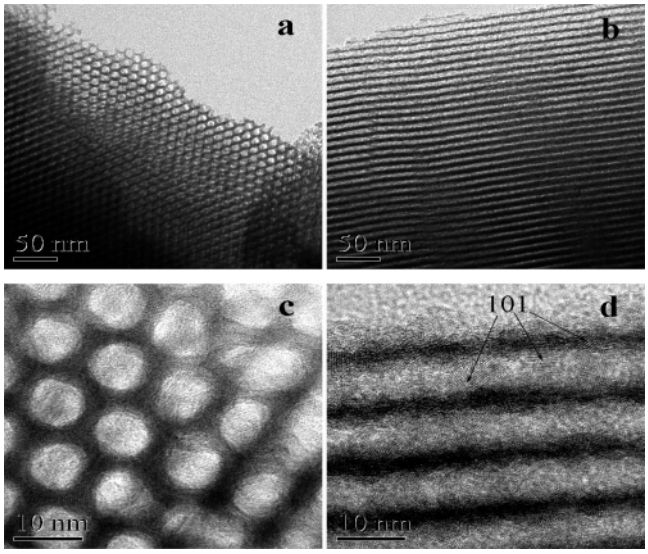

Figure 3. TEM (a, b) and HRTEM (c, d) images of ordered mesoporous TiO_2 calcined at 350 °C for 6 h, viewed along [001] (a, c) and [110] (b, d) directions.

p_0) of ~0.7 (Figure 4Aa), suggesting a very narrow pore size distribution. The hysteresis loop is a very close H1 type, implying a uniform cylindrical pore geometry.[10,23] The pore size calculated from the adsorption data using the BJH model is as large as 7.6 nm (Figure 4Ba). The pore wall thickness calculated from the pore size and unit cell is about 4.3 nm, which is essentially consistent with that evaluated from TEM images. The calculated BET specific surface area is as high as 271 m^2/g. Considering the large density of titania (4.2 g/cm^3), this value is commensurate with that for mesoporous silica prepared from the EISA method (Table 1). After being calcined at 400 °C in air, the mesoporous TiO_2 products show a sharp capillary condensation step with a little wide relative pressure range of 0.5−0.65 (Figure S4), suggesting a narrow mesopore size distribution. The calculated mean size is ~6.3 nm, which is a little smaller than that of the sample calcined at 350 °C. It is worth noting that the hysteresis loop of the isotherms changes to the H2 type,[23] suggesting an ink bottle pore.[10,23] It is caused by the pore blocking from the thrust of large anatase nanocrystallites,[10,23] which is in agreement with the observation from TEM. The calculated BET surface area is still high (213 m^2/g). After further being calcined at 450 °C, the mesoporous TiO_2 has a still high BET specific surface area (171 m^2/g) and pore volume (0.26 cm^3/g) (Table 1); however, the pore size distribution becomes wide (Figure S5), indicating that the mesostructure is greatly degraded.

Mesoporous Titania−Silica Composites. Highly ordered mesoporous titania−silica composites can be synthesized by the synchronous assembly strategy based on the EISA method under a large amount of HCl dependent on the Ti/Si ratio by using P123 as a template. SAXRD patterns (Figure 1A) of all as-synthesized TiO_2-SiO_2 composites with different Ti/Si ratios show three well-resolved diffraction peaks indexed as the 100, 110, and 200 reflections, respectively, suggesting a typical 2-D hexagonal mesostructure. The calculated a_0 parameters increase with Ti/Si ratio increase, probably due to large titania clusters aggregated. After being calcined at 350−450 °C in air to remove the template, three well-resolved diffraction peaks can still be observed (Figure 1B), clearly indicating that the highly ordered 2-D hexagonal mesostructures are thermally stable. The calculated structural shrinkages are in the range of 14−21% and a little increase with the Ti/Si ratio, which are a little smaller than that (26%) of mesoporous TiO_2 calcined at 400 °C. It implies that the compact degree of the frameworks is slightly higher than that of the mesoporous pure TiO_2.

Similar to that of the pure titania, WAXRD patterns (Figure 2) of the mesoporous TiO_2-SiO_2 composites after being calcined at 450 °C to remove the templates display the characteristic diffraction peaks of anatase phases, indicating a formation of TiO_2 nanocrystals. With the increase in the TiO_2/SiO_2 ratio, the intensities of the diffractions increase, indicating that the crystallinity of anatase nanocrystals enhances. It further suggests that amorphous SiO_2 in the pore walls may inhibit the crystallization of TiO_2. The size of TiO_2 nanocrystals in the framework matrixes is calculated to be in the range of 4−4.9 nm and increases with Ti/Si ratio, which is smaller than that (6.5 nm) of mesoporous TiO_2 (Table 1).

TEM images further confirm that mesoporous TiO_2-SiO_2 composites with a variable Ti/Si ratio from 0 to ∞ have a highly ordered 2-D hexagonal regularity (Figures 5 and S6−S8). The cell parameters evaluated from TEM measurements are in the range of 11.0−12.4 nm, which increase a little with the increase in the Ti/Si ratio. It is consistent with the trend obtained from the SAXRD patterns (Table 1). HRTEM images (Figures 5c,d and S6−S8) reveal that anatase nanocrystals connected by the amorphous mortars are randomly oriented and overlap each other on the pore walls. The lattice fringe can clearly be observed in HRTEM images with the average *d*-spacing of 0.34 nm, which is indexed as the 101 reflection of the anatase structure. It agreed with the d_{101} spacing calculated from the corresponding WAXRD patterns. The average size of anatase nanocrystals evaluated from the HRTEM images is in the range of 6−13 nm, which increases with the increase in the Ti/Si ratio. It agrees with the trend from XRD measurements. Some of the anatase nanocrystals pierce into and block the channels; however, they are still linked with amorphous mortars. The pore

(23) Kruk, M.; Jaroniec, M. *Chem. Mater*. **2001**, *13*, 3169−3183.

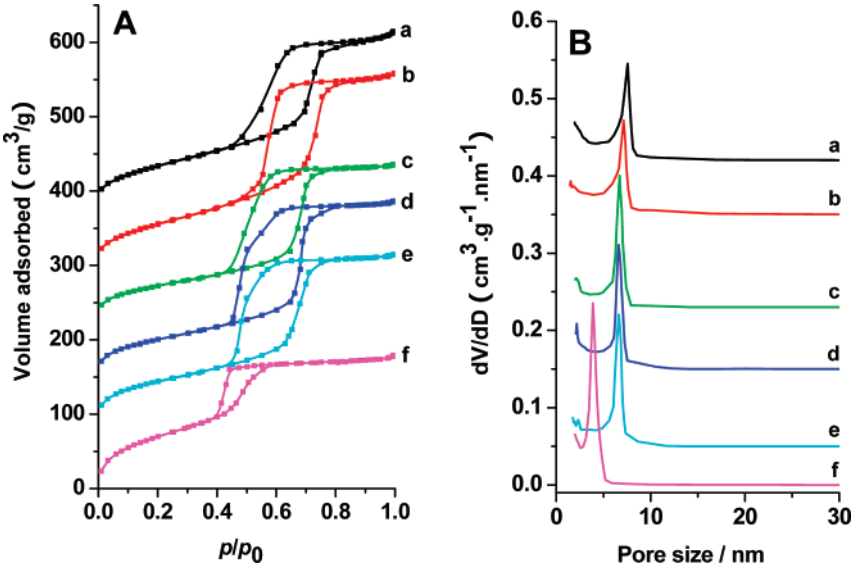

Figure 4. (A) N_2 adsorption−desorption isotherms and (B) pore size distributions of (a) ordered hexagonal mesoporous TiO_2 calcined at 350 °C for 6 h; (b) mesoporous $90TiO_2$−$10SiO_2$, (c) $80TiO_2$−$20SiO_2$, (d) $70TiO_2$−$30SiO_2$, and (e) $60TiO_2$−$40SiO_2$ composites calcined at 450 °C for 4 h; and (f) mesoporous SiO_2 sample calcined at 600 °C for 4 h in air. The isotherms a−f are offset vertically by 360, 275, 210, 130, 65, and −50 cm^3/g, respectively.

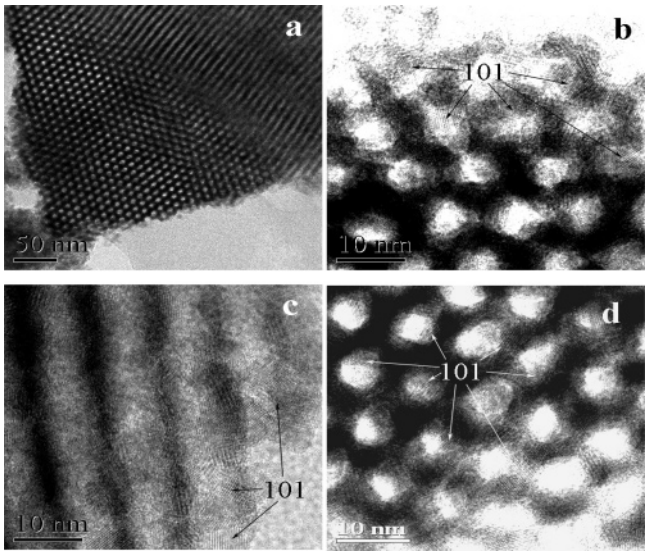

Figure 5. TEM (a) and HRTEM (b−d) images of ordered 2-D hexagonal mesoporous $80TiO_2$−$20SiO_2$ composite calcined at 700 °C for 4 h (a−c) and 800 °C for 2 h (d), viewed along [001] direction (a, b, and d) and [110] direction (c).

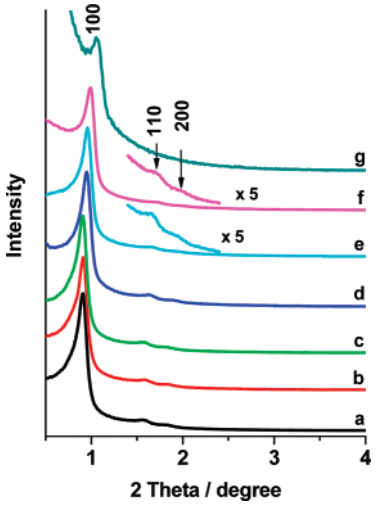

Figure 6. SAXRD patterns of the highly ordered hexagonal mesostructured $80TiO_2$−$20SiO_2$ composites calcined at 600 °C for 4 h (a), 650 °C for 4 h (b), 700 °C for 4 h (c), 750 °C for 2 h (d), 800 °C for 2 h (e), 850 °C for 2 h (f), and 900 °C for 2 h (g).

wall thickness can roughly be evaluated from the HRTEM images to be in the range of 4.4−5.3 nm, which decreases with the decrease in the Ti/Si ratio.

N_2 adsorption−desorption isotherms of mesoporous TiO_2−SiO_2 composites with various Ti/Si ratios after the removal of the templates exhibit characteristic type IV curves with sharp capillary condensation steps at relative pressure (p/p_0) of ∼0.7, suggesting well-uniform mesopores (Figure 4A,B). The hysteresis loops are very close to the H1 type, suggesting a uniform cylindrical pore geometry.[10,23] The pore sizes calculated from the adsorption data using the BJH model are in the range of 6.6−7.1 nm (Table 1), increasing with the increase in the Ti/Si ratio. The half-height width of the pore size distribution is in the range of 0.73−0.76 nm (Table 1), indicating a very narrow pore size distribution. The BET specific surface area is as high as 251−380 m^2/g, increasing with the decrease in the Ti/Si ratio (Table 1). It is mainly related to the low density resulted from the silica incorporation and mesostructural regularity. The calculated pore wall thickness is in the range of 4.2−5.5 nm, increasing with the Ti/Si ratio, which is in agreement with the TEM observations.

Thermal Stability of Mesoporous Titania−Silica Composites. To investigate the thermal stability, all resulting mesoporous TiO_2−SiO_2 composites were calcined at 500−900 °C for 2−4 h in air with an interval of 50 °C. Here, we chose the representative composites with Ti/Si ratio of 80/20 as an example to demonstrate the stability functioned with the calcination temperature.

SAXRD patterns of mesoporous $80TiO_2$−$20SiO_2$ composites show three resolved diffraction peaks after being calcined at 600−850 °C, indicating that the composites are highly thermally stable (Figure 6). With the increase in calcination temperature, the diffraction intensity decreases and the width of the peaks increases, suggesting that the mesostructures degrade a little. It

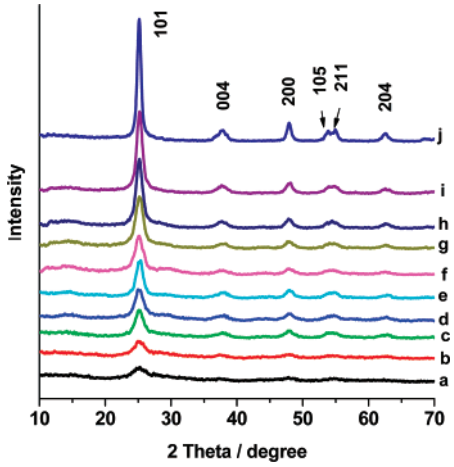

Figure 7. WAXRD patterns of the highly ordered hexagonal mesoporous $80TiO_2-20SiO_2$ composites calcined at 350 °C for 6 h (a), 450 °C for 4 h (b), 550 °C for 4 h (c), 600 °C for 4 h (d), 650 °C for 4 h (e), 700 °C for 4 h (f), 750 °C for 2 h (g), 800 °C for 2 h (h), 850 °C for 2 h (i), and 900 °C for 2 h (j).

is mainly related to the growth of anatase nanoparticles. When the temperature reaches 900 °C, only one diffraction peak can be observed, suggesting that the regularity of the hexagonal mesostructure is largely damaged. TEM measurements further confirm that the mesoporous $80TiO_2-20SiO_2$ composites are poorly ordered in most domains (Figure S9). Therefore, 900 °C is the threshold of the thermal stability for the mesoporous $80TiO_2-20SiO_2$ composite structure. Similar trends are observed for mesoporous TiO_2-SiO_2 composites with various Ti/Si ratios; however, the threshold temperature is a little different. When the silica is incorporated into the composites, the thermal stability of the mesostructure is greatly enhanced (Figures S10−S12), compared with that for mesoporous pure TiO_2 (the threshold is about 450 °C, Figures S1 and S3). It suggests that amorphous silica plays a key role for the improvement of the thermal stability. Our XRD, TEM, and N_2 sorption isotherm results show that, when the Ti/Si ratio is higher than 90/10, the composites can be stable around 700 °C. For example, the threshold for the mesoporous $90TiO_2-10SiO_2$ composite is about 750 °C. When the Ti/Si ratio is lower than 80/20, the stability of mesoporous TiO_2-SiO_2 composites greatly increases to around 900 °C. It is the highest stability reported up to now for ordered mesoporous TiO_2-SiO_2 composites when the titania content is higher than 50%. It implies that the silica amorphous mortar is enough for the stabilization of the mesostructure. When the silica content is higher than 50%, the thermal stability for the ordered mesostructure of TiO_2-SiO_2 composites is not significantly changed with the Ti/Si ratio, which is similar to that for mesoporous silica.

WAXRD patterns of mesoporous $80TiO_2-20SiO_2$ composites calcined at different temperatures (Figure 7) show that the anatase nanocrystals are formed at 350 °C. With the increase in temperature, the diffraction intensities of the anatase phase are enhanced greatly, indicating that the crystallinity and the particle size increase. After being calcined at 900 °C, the average size of the anatase nanocrystals is calculated from Scherrer's formula to be 12.5 nm, which is two times larger than the thickness of the pore walls (Table 1). It implies that such sized anatase nanocrystals may occupy the whole channels, resulting in a collapse of the mesostructure. HRTEM measurements further confirm this conclusion (Figure S9). The average size of anatase nanocrystals is about 13 nm measured from the TEM images, and most of them overlap each other. Large areas of the channels are filled by the large anatase nanocrystallites.

With the increase in the Ti/Si ratio, WAXRD patterns of the mesoporous TiO_2-SiO_2 composites (Figures S10B, S11B, and S12B) show that the formation temperature of anatase phases is about 350 °C, which is independent of the ratio, suggesting a relation to TiO_2 phase intrinsical features. With the increase in temperature, the particle size of the anatase nanocrystals greatly increases similar to that for $80TiO_2-20SiO_2$ composites. Our results based on TEM and WAXRD measurements show that the temperature required forming the same size of TiO_2 nanocrystals is different. The higher the Ti/Si ratio, the lower the temperature. It further suggests that the thermal stability of the nanocomposites can be greatly improved by incorporating the silica content.

N_2 sorption measurements show that the pore size of mesoporous $80TiO_2-20SiO_2$ composites decreases with calcination temperature (Figure 8A,B, Table 1). When the temperature is lower than 750 °C, the hysteresis loop of the isotherms is close to the H1 type. When temperature is higher than 800 °C, the loop changes to the H2-like type, suggesting a change from cylindrical to ink bottle shaped mesopore channels.[10,23] This is caused by the growth of anatase nanocrystallites. The large TiO_2 nanocrystals can thrust into the cylindrical channels and partially block the pores, which can be clearly seen from the HRTEM image (Figure 5d), resulting in the formation of ink bottle shaped pores. Especially, as seen in Figure 8Af, the drop of the desorbed amount in the p/p_0 region of 0.4 to 0.5 is relatively sharp, which is characteristic for the H2 hysteresis loop. Since the size of anatase TiO_2 nanocrystals gradually increases with calcination temperature, the blockage of pore openings increases, and therefore the hysteresis loop gradually changes from H1 to H2 type.

With the increase in the calcination temperature, the BET surface area and pore volume decrease gradually and the pore wall thickness increases (Table 1). The threshold temperature can be found to be about 900 °C. After being calcined at such temperature, the BET surface area and pore volume are only 73 m^2/g and 0.08 cm^3/g, respectively, clearly indicating the block of the channels and a collapse of the mesostructure. It agrees with the results from XRD and TEM measurements (Figure S9).

With varied Ti/Si ratios, a similar trend that the BET surface area and pore volume decrease and the pore wall thickness increases with rising temperature can be obtained (Table 1). The different transformation temperature from the H1 type hysteresis loop to the H2 type is observed (Figures S13−S15). With Ti/Si ratio increase, the temperature appearance H2 hysteresis loop decreases. The threshold temperature is about 750 °C when the Ti/Si ratio is higher than 80/20, and the temperature is higher than 900 °C when the Ti/Si ratio is lower than 80/20. This indicates that incorporating more SiO_2 content in the frameworks can result in higher thermal stability.

Formation of Mesostructures. Using TIPO as a titania source, TEOS as a silica source, and P123 as a template, we could successfully synthesize via an ethanolic EISA process a series of highly ordered hexagonal mesoporous TiO_2-SiO_2 composites with variable Ti/Si ratios. Our results show that the formation of mesostructured TiO_2-SiO_2 nanocomposites un-

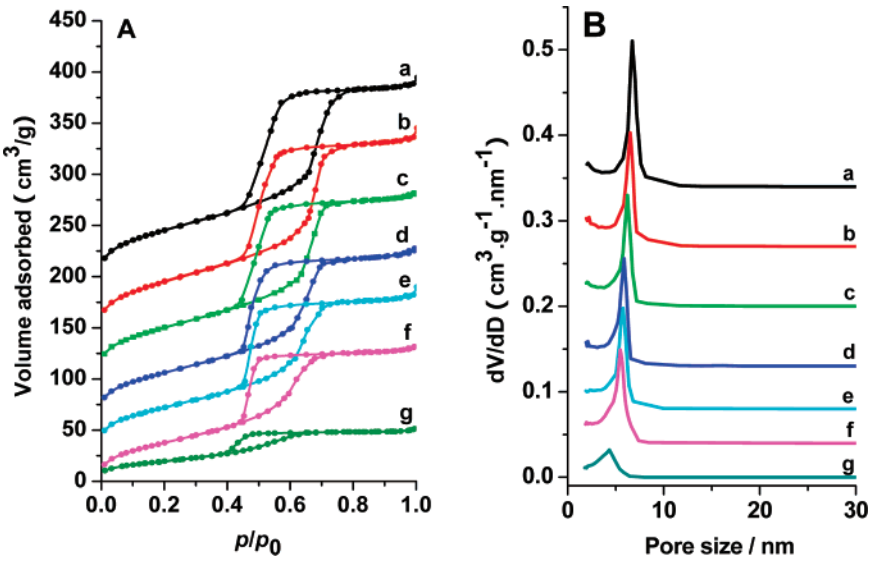

Figure 8. N_2 adsorption−desorption isotherms (A) and pore size distributions (B) of the highly ordered hexagonal mesoporous $80TiO_2-20SiO_2$ composites calcined at 600 °C for 4 h (a), 650 °C for 4 h (b), 700 °C for 4 h (c), 750 °C for 2 h (d), 800 °C for 2 h (e), 850 °C for 2 h (f), and 900 °C for 2 h (g). The isotherms a−f are offset vertically by 180, 130, 90, 50, 20, and −10 cm^3/g, respectively.

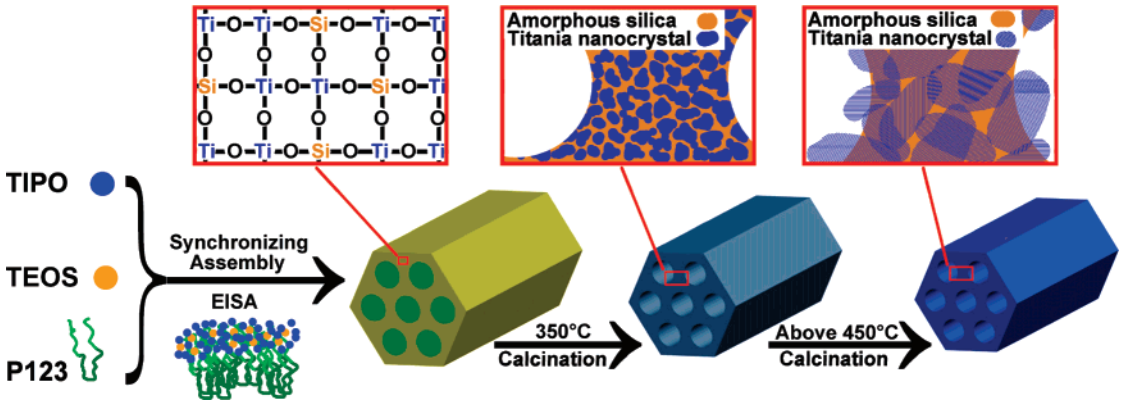

Figure 9. Scheme for the synchronous assembly of titanate oligomers from TIPO and silicate species from TEOS molecules with triblock copolymer P123 template to form highly ordered mesoporous anatase nanocrystalline TiO_2-SiO_2 composites.

dergoes a co-self-assembly process of titanate oligomers hydrolyzed from TIPO, silicate oligomers from TEOS, and amphiphilic triblock copolymer P123. The final nanocomposites have a uniform and homogeneous framework with well-dispersed silicates, in which both silicate and titanate oligomers can cross-link together and contribute the mesostructured frameworks without phase separation (Figure 9). Our results demonstrate that the synchronicity of the condensation and polymerization rates of TIPO and TEOS molecules during the EISA process and co-assembly with P123 template molecules is a key factor to successful organization of highly ordered composite mesostructures. It is known that the cross-linking rate for TIPO is much faster than that for TEOS, which can be slowed down by high acidity. The acidity is a good catalyst for the hydrolysis and condensation of silicate species. In this case, we adopted the adding large HCl acidity amount approach to simultaneously lower the condensation and polymerization rates of TIPO and accelerate the rates for TEOS. It is proven that the method is controllable and repeatable to successful organization of highly ordered composite mesostructures with a wide range of Ti/Si ratios (0 to ∞).

Although a large amount of HCl was used in our synthesis, the amount of the acidity (HCl) required varies according to the Ti/Si ratio, because of the largely different hydrolysis and polymerization rates of TIPO and TEOS. It is very important for the synchronous assembly of the titanate and silicate oligomers with P123 templates. With the decrease in the Ti/Si ratio, the range of required HCl amount narrows. For example, when the Ti/Si ratio is higher than 80/20, the highly ordered hexagonal mesostructured TiO_2, $90TiO_2-10SiO_2$ and $80TiO_2-20SiO_2$ composites can be obtained within a wide range of 1.5−3.0 g of concentrated HCl in 1.0 g of P123 system (Figure S16). With the increase in TEOS amount, the required amount of concentrated HCl decreases. The highly ordered $70TiO_2-30SiO_2$ composite mesostructure was obtained within 1.5−2.2 g of concentrated HCl (Figure S17). The $60TiO_2-40SiO_2$ composite with highly ordered hexagonal mesostructure was obtained in the conditions of 1.5−1.8 g of concentrated HCl (Figure S18).

In addition, to synchronize the assembly of the titanate and silicate oligomers with P123 molecules, the relative humidity of the surrounding atmosphere and the evaporation temperature should also be finely tuned corresponding to the Ti/Si ratio. With the decrease in the Ti/Si ratio, the relative humidity increases and the evaporation temperature is enhanced, which can offset the decrease in the HCl amount. We adopted 50−

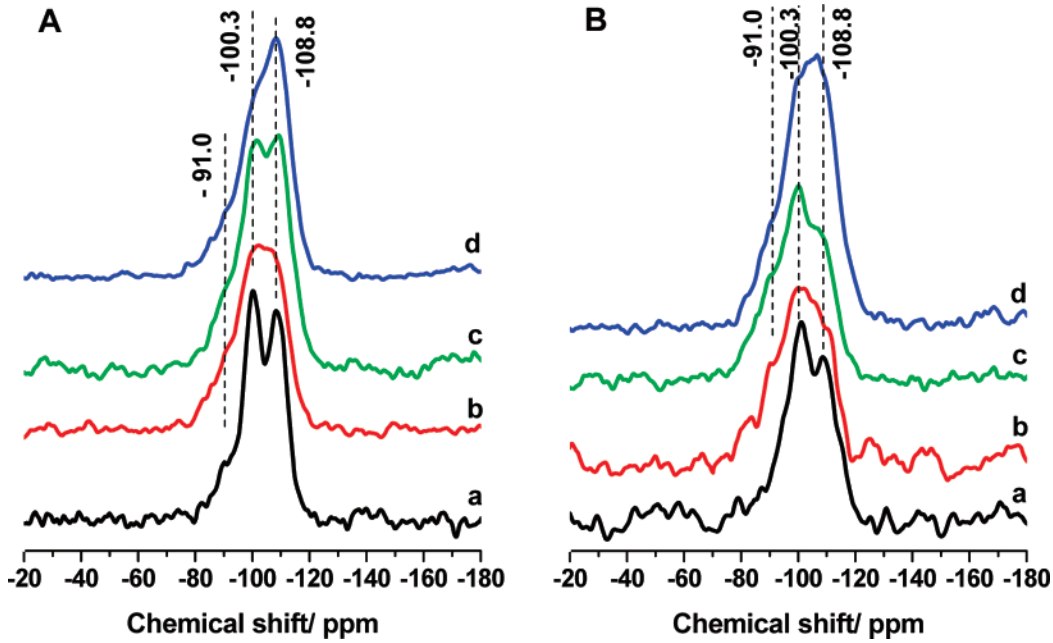

Figure 10. ^{29}Si MAS NMR spectra of the highly ordered 2-D hexagonal mesostructured $60TiO_2-40SiO_2$ (A) and $80TiO_2-20SiO_2$ (B) composites. (a) As-made. (b−d) Calcined at 400 °C for 6 h, 600 °C for 4 h, and 800 °C for 2 h, respectively.

60% relative humidity and evaporation temperature of 35 °C for the synthesis of mesoporous TiO_2, $90TiO_2-10SiO_2$ and $80TiO_2-20SiO_2$ composites. The highly ordered hexagonal mesostructured $70TiO_2-30SiO_2$ composite was obtained within 65−80% of relative humidity at 35 °C. The ordered $60TiO_2-40SiO_2$ composite mesostructure was obtained within 65−80% of relative humidity at 40 °C.

Upon calcination at 350 °C, the template can be removed and the mesopores are liberated. Simultaneously, the titanate species are aggregated and the homogeneous amorphous frameworks start to crystallize because of the thermodynamic metastability of TiO_2 during the heat treatment.[9] The nuclei and nanocrystals of TiO_2 are formed in the pore walls. At this moment, the phase separation occurs and anatase TiO_2 nanocrystals are randomly embedded in the matrixes of amorphous TiO_2 and SiO_2. As the temperature increases and/or the heat treatment time prolongs, the phase separation continues to progress and the TiO_2 nanocrystals further grow. At this stage, the nanosized anatase domains and the nanosized SiO_2-rich phase domains form. Fortunately, the silica domains keep being amorphous during the process, which serves as a glue to make those anatase nanocrystals connected to each other, retaining the ordered mesostructures. On the other hand, the amorphous silica framework domains can prevent the titanate species aggregating together and further coarsening into large nanocrystals, which makes the frameworks avoid collapsing. The more the silica content, the smaller the size of TiO_2 nanocrystals, and the higher the thermal stability. When the nanocrystals have the dimension size comparable to the pore wall thickness, which enables the nanocrystals to penetrate the mesochannels, the mesostructure is still retained. When the size is larger than 2 times the pore wall thickness, the main channels can be fully occupied, and the mesostructure would completely collapse. In the mesoporous TiO_2's case, amorphous TiO_2 can also act as the glue to maintain the mesostructure regularity under 350−400 °C. Upon calcination at 450 °C, the amorphous TiO_2 can fully transform into crystalline TiO_2 and the mesostructure completely collapses.

^{29}Si solid-state MAS NMR spectra can provide further information about the formation of the mesostructure and the pore wall structure (Figure 10). The as-made mesoporous $60TiO_2-40SiO_2$ composite shows three resonance bands at around −108.8, −100.3, and −91.0 ppm with the relative areas of 42, 43, and 15%, respectively (Figure 10Aa). These bands can be attributed to $[(TO)_4Si, Q^4]$, $[HO-Si(OT)_3, Q^3]$, and $[Si(OT)_2(OH)_2, Q^2]$,[24] respectively, where T can be Si or Ti. An intense Q^4 band is observed for the as-made nanocomposite, implying that silicate oligomers can cross-link with dominated titanate species to contribute the mesostructured frameworks; otherwise the minor silicates would yield large amounts of Q^2 or Q^3 bands. It is interesting that, after the calcination at 400 °C to remove the templates, the three bands can still be observed and the ratio of Q^4 to Q^3 does not change much (Figure 10Aa,b). With the further increase in calcination temperature, the Q^4/Q^3 ratio slightly increases (Figure 10Ac,d). These phenomena are much different from that for mesoporous silicates; the latter show a large increase in the Q^4/Q^3 ratio, because during the thermal process silicates can further cross-link. The results suggest that the interaction between silicates and titanate species is weak. After the calcination at high temperature, the Si−O−Ti bonds can be disassociated and the microphase separation occurs. Similar cases can be observed for mesoporous $80TiO_2-20SiO_2$ nanocomposites (Figure 10B).

Photocatalytic Performance. The photocatalytic activities for resulting mesoporous TiO_2-SiO_2 composites were evaluated by the degradation of RhB solution under UV light irradiation. For comparison, the photocatalytic activity of commercial nonporous photocatalyst P25 was also measured under the same condition. The weight for all the samples is exactly the same. Figure 11A shows the time profiles of C/C_0 under UV light irradiation for the representative samples with variable Ti/Si

(24) Kang, M.; Hong, W. J.; Park, M. S. *Appl. Catal., B* **2004**, *53*, 195−205.

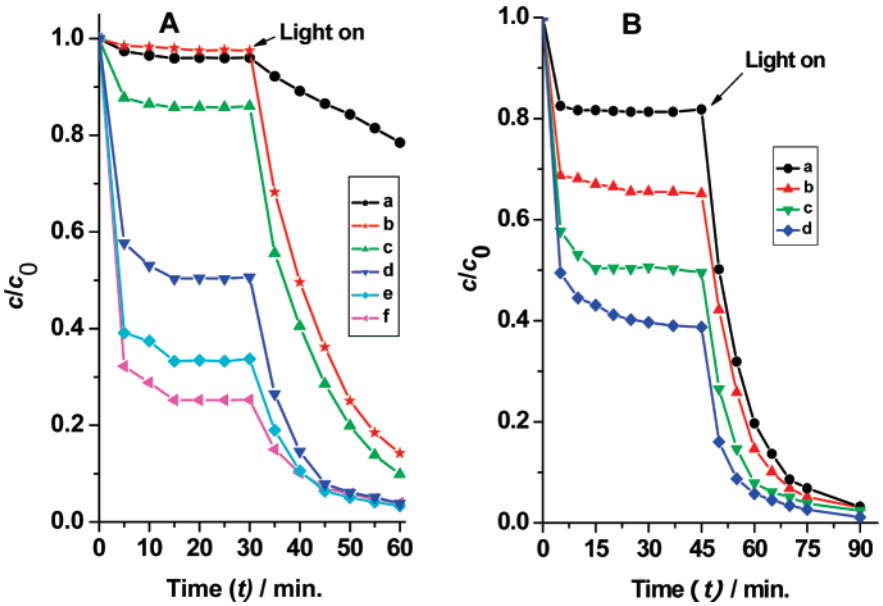

Figure 11. Photocatalytic degradation of RhB monitored as the normalized concentration change versus irradiation time in the presence of (A) mesoporous TiO_2-SiO_2 composites prepared with different Ti/Si ratios. (a) Mesoporous TiO_2 calcined at 400 °C for 2 h; (b) commercial photocatalyst P25; (c) mesoporous $90TiO_2-10SiO_2$ composite calcined at 700 °C for 2 h; (d) mesoporous $80TiO_2-20SiO_2$, (e) $70TiO_2-30SiO_2$, and (f) $60TiO_2-40SiO_2$ composites calcined at 850 °C for 2 h. (B) Photocatalytic degradation for mesoporous $80TiO_2-20SiO_2$ composites calcined at 700 °C for 4 h (a), 800 °C for 2 h (b), 850 °C for 2 h (c), and 900 °C for 2 h (d).

ratios, respectively, where C is the concentration of RhB at the irradiation time t and C_0 is the initial concentration. The corresponding rate constants were calculated as shown in Figure S19. For easier understanding, the adsorption process and photocatalytic reaction are separately discussed. Before light on, an adsorption process of RhB in the pores occurs. The adsorption proceeds very fast, which is close to saturation within 5 min and reaches equilibrium within ~15 min. The adsorption amount of RhB on the mesoporous materials is higher than that on P25, because the former have much larger surface areas. With the decrease in the Ti/Si ratio, the adsorption amount of RhB increases, which agrees with the increase in the surface area. After light on, the concentration of RhB decreases fast with the irradiation time and the pseudo-first-order reaction is observed (Figure S19). Compared with that of the commercial P25 (Figures 11Ab and S19Ab, $k_b = 0.0671$ min^{-1}), the mesoporous pure TiO_2 calcined at 400 °C shows slower decomposition rate and catalytic activities (Figures 11Aa and S19Aa, $k_a = 0.00648$ min^{-1}), probably due to the lower anatase crystallinity in the frameworks. The mesoporous $90TiO_2-10SiO_2$ composite calcined at 700 °C ($k_c = 0.0720$ min^{-1}) and the mesoporous composites of $80TiO_2-20SiO_2$ ($k_d = 0.109$ min^{-1}), $70TiO_2-30SiO_2$ ($k_e = 0.0976$ min^{-1}), and $60TiO_2-40SiO_2$ ($k_f = 0.0841$ min^{-1}) calcined at 850 °C, respectively, exhibit higher photocatalytic activities (Figures 11Ac,d,e,f and S19Ac,d,e,f) than P25, which may be attributed to their higher surface areas and larger pore volumes. More interestingly, when the Ti/Si ratio is fixed (e.g., 80/20), both the adsorption performance and the activity increase with the increase in the calcination temperature (Figures 11B and S19B, $k = 0.0903-0.109$ min^{-1}), which are higher than that of P25, implying that it is mainly dependent on their crystallinity of anatase nanocrystals and the BET surface area. The mesoporous TiO_2-SiO_2 composites exhibit a binary function for the degradation of RhB derived from their high surface areas and highly crystalline anatase nanoparticles. Large surface areas and pore volumes can enrich RhB molecules in the channels to contact with anatase nanocrystals which act as the catalytic sites to degrade the molecules under UV light irradiation. This unique feature makes the composites exhibit excellent photodegradation activity.

Conclusions

The highly ordered 2-D hexagonal mesoporous TiO_2-SiO_2 composites with variable Ti/Si ratios (0 to ∞) have been successfully synthesized using TIPO as a titania source, TEOS as a silica source, and triblock copolymer P123 as a template via a synchronous assembly approach based on an ethanolic EISA process. XRD, TEM, and N_2 sorption techniques have been used to systematically investigate the pore wall structure and thermal stability. The results showed that the resultant materials have ultrahigh stability, large uniform pore size, and high BET surface areas. The highly ordered mesoporous TiO_2 with 2-D hexagonal structure can be obtained by adding a large amount of acid HCl under low relative humidity and evaporation temperature. The obtained mesoporous TiO_2 products have large uniform pore size (~7.6 nm) and high surface area (271 m^2/g). Upon calcination at 350 °C, the amorphous frameworks can transform to semicrystalline anatase pores and walls. The TiO_2 mesostructure can be thermally stable at 450 °C. The highly ordered mesoporous TiO_2-SiO_2 composites with Ti/Si ratios of 90/10, 80/20, 70/30, and 60/40 can be obtained by finely tuning the relative humidity and evaporation temperature. With the decrease in the Ti/Si ratio, the adopted relative humidity and evaporation temperature increase. The obtained TiO_2-SiO_2 composites show highly ordered 2-D hexagonal mesostructures, large uniform pore size (5.0−7.1 nm), high BET surface areas (190−308 m^2/g), and large pore volume (0.22−0.43 cm^3/g). The pore size and pore volume decrease with the increase in calcined temperature and the decrease in the Ti/Si ratio. The thermal

stability is greatly improved with incorporated amorphous silica. With the decrease in the Ti/Si ratio, the stability enhances. The $90TiO_2-10SiO_2$ composite can be stable at 750 °C. When the Ti/Si ratios are ≤80/20, the stability of the composite mesostructures is higher than 900 °C. During the calcination, titania is fully crystalline to form anatase nanocrystals, which are uniformly embedded in the pore walls to form "bricked mortar" frameworks. The amorphous silica acts as a glue linking the TiO_2 nanocrystals and improves the thermal stability. With the increase in calcination temperature, the size of anatase nanocrystals increases in the range of 4−12 nm. With the decrease in the Ti/Si ratio, the TiO_2 nanocrystal size decreases, because the silica framework domains can prevent the titanate species from aggregating and further coarsening, and the frameworks from collapsing. Our strategy is the synchronicity of the self-assembly of titanate and silicate oligomers with triblock copolymer P123 by adding a large amount of HCl acidity. It can lower the condensation and polymerization rates of TIPO and accelerate the rates for TEOS molecules. Our results demonstrate that this synchronous assembly approach is controllable and repeatable. The mesoporous nanocomposites exhibit excellent photocatalytic activities, which are higher than that for commercial catalyst P25, for the degradation of RhB in aqueous suspension. With the increase in calcination temperature, the photocatalytic activities are enhanced. It is ascribed to the bifunctional effect of the crystalline anatase nanoparticles and high porosity.

Acknowledgment. This work was supported by the Start-up Research Fund for Returning Scholars from the Education Ministry of China (KEH1829028), NSFC (20421303, 20521140450), State Key Basic Research Program of PRC (2006CB932302), Shanghai Sci. & Tech. Committee (06DJ14006, 05DZ22313), and Shanghai Nanotech Promotion Center (0652nm024). W.D. thanks the Korean Federation of Science and Technology Societies for an International Visiting Scholar supported through the Brain-Pool Program. We also thank Dr. H. F. Yang, Dr. J.-O. Baeg, Mr. T. H. Jin, Mr. J.-N. Park, Prof. Y. Tang, T. L. Wu, Y. H. Yue, and Dr. S. H. Xie for helpful discussion and characterization assistance.

Supporting Information Available: Other related SAXRD and WAXRD patterns, TEM and HRTEM images, figures of N_2 adsorption−desorption isotherms, and pore size distributions. This material is available free of charge via the Internet at http://pubs.acs.org.

JA073804O